

January 9, 2004

Radio Observations of Rapid Acceleration in a Slow Filament Eruption/Fast CME Event

M. R. Kundu¹, S. M. White¹, V. I. Garaimov¹, P. K. Manoharan², P. Subramanian³, S. Ananthkrishnan⁴, and P. Janardhan⁵

¹*Astronomy Department, University of Maryland, College Park, MD 20742*

²*Department of Physics, Catholic University of America, Washington DC 20064*

³*Inter-University Centre for Astronomy and Astrophysics, P.O. Bag 4, Ganeshkhind, Pune-411007, India*

⁴*National Centre for Radio Astrophysics, TIFR, P. O. Bag 3, Ganeshkhind, Pune-41007, India*

⁵*Physical Research Laboratory, Astronomy & Astrophysics Division, Navrang-pura, Ahmedabad-380009, India*

ABSTRACT

We discuss a filament eruption/coronal mass ejection (CME) event associated with a flare of GOES class M2.8 that occurred on November 17, 2001. This event was observed by the Nobeyama RadioHeliograph (NoRH) at 17 and 34 GHz. NoRH observes the filament during its eruption both as a dark feature against the solar disk and a bright feature above the solar limb. The high cadence of the radio data allows us to follow the motion of the filament at high time resolution to a height of more than half a solar radius. The filament eruption shows a very gradual onset and then a rapid acceleration phase coincident with the launch of a fast halo CME. Soft X-ray and EUV images show heating in a long loop underneath the filament prior to the flare. The NoRH height-time plot of the filament shows a roughly constant gradual acceleration for an hour, followed by a very abrupt acceleration coincident with the impulsive phase of the associated flare, and then a phase of constant velocity or much slower acceleration. This pattern is identical to that recently found to occur in the motion of flare-associated CMEs, which also show a sharp acceleration phase closely tied to the impulsive phase of the flare. When the rapid acceleration occurs in this event, the flare site and the filament are separated by about $0.5 R_{\odot}$, making it unlikely that a disturbance propagates from one location to the other. Models in which a disruption of the large-scale coronal magnetic field simultaneously permits the acceleration of the filament and the flare energy release seem to be a better explanation for this event.

Subject headings: Sun: flares – Sun: corona – Sun: radio radiation

1. INTRODUCTION

The close connection between filament eruptions and coronal mass ejections has long been recognized (Webb et al. 1976; Munro et al. 1979; Kahler et al. 1988), although there continues to be a healthy debate about the degree of association between the two phenomena (Wang & Goode 1998; Gilbert et al. 2000; Gopalswamy et al. 2003). A typical CME eruption is now believed to possess a three-part structure (Illing & Hundhausen 1986): an outer rim carrying the bulk of the ejected material at the highest speed, followed by a cavity that is dark in coronagraph images but is believed to carry intense magnetic field strengths, and then by the filament material that is generally travelling at speeds slower than the outer front.

Filaments (called prominences when viewed as emission features above the limb, but we will use the term filament throughout this paper) are most commonly studied with H α observations in the visible range since filaments readily appear as absorption features against the chromospheric emission at that wavelength, while coronal mass ejections are generally viewed with white-light coronagraphs. But radio observations have also proven to be a powerful technique for the study of filaments: at microwave frequencies they show up as dark absorption features (10^4 K against a background disk of $> 2 \times 10^4$ K), and they are also visible as emission features above the limb as long as they remain optically thick at radio wavelengths (Kundu 1970; Drago & Felli 1970; Kundu 1972; Chiuderi-Drago et al. 1975; Chiuderi Drago 1990). In particular, they are readily visible in 17 GHz images from the Nobeyama Radioheliograph (Hanaoka et al. 1994; Gopalswamy & Hanaoka 1998), which cover the full disk with a resolution of order $12''$ and are available at a cadence of 1 second for 8 hours every day. This data set is a powerful resource for the study of filaments and their eruption, as demonstrated by Gopalswamy et al. (2003) in a study of 186 prominence eruptions: the erupting material can be followed up to heights well above the solar surface, as far as $2.5 R_{\odot}$.

As noted above, in most CME/filament eruption events the filament material lags well behind the leading edge of the CME, and its behaviour is not necessarily the same as the behaviour of the CME itself. The relationship between an erupting filament and any associated CME is an ongoing area of study, particularly for the issue of causality: does the filament eruption drive the CME, or does the CME release the filament, or are both features consequences of something else? This issue is important for understanding the dynamics of CMEs with their potential to cause space weather effects. In this paper we study an interesting CME/filament eruption event in which the NoRH radio data allow us to study the height-time behaviour of the filament over several hours. We identify the occurrence of a period of high acceleration that coincides with the impulsive phase of

the associated solar flare, well after the initial rise of the filament. This event was well observed by a wide range of telescopes and hence a comprehensive set of diagnostics is available: the NoRH at 17 GHz and 34 GHz, radio patrol telescopes, the Soft X-ray Imager (SXI) on the GOES 12 satellite, and the Extreme-ultraviolet Imaging Telescope (EIT), Michelson Doppler Imager (MDI) and Large Angle Spectroscopic Coronagraph (LASCO) experiments on the SOHO spacecraft. In addition, this event was one of the first solar flares to be observed with the the Giant Meterwave Radio Telescope (GMRT) in India, which was operating in the 1 GHz band at the time. An analysis of the event focussing on the GMRT data was presented by Subramanian et al. (2003). Here we focus more on the associated filament eruption that was well observed by NoRH, and investigate how it fits into recent analyses of CMEs.

2. FILAMENT ACTIVATION

The event starts with the gradual outward motion of a filament in the south-east quadrant of the Sun. The filament that erupts in this event is shown in Figure 1. The panels show $H\alpha$, He 304 Å and Fe XII 195 Å images spanning about 5 hours prior to the event. In the $H\alpha$ image the filament is quite large, and located over $100''$ to the north-east of the closest active region, AR 9704 at S18E41. The filament was quite stable until some time after 03:30 UT: the final image in Fig. 1 shows definite outwards motion that is first visible by comparing successive EIT images taken at 03:24 and 03:48 UT.

The cadence of the EIT 195 Å images is not adequate to follow the motion of the filament in detail, but fortunately it is also a prominent feature of the NoRH images. At 17 and 34 GHz the solar disk has a brightness temperature of order 10000 K, and dense filaments may appear as depressions of brightness temperature against the disk because they are optically thick at a temperature lower than this, typically 5000 – 7000 K (Kundu 1972; Chiuderi Drago 1990; Gopalswamy & Hanaoka 1998; Hanaoka & Shinkawa 1999; Chiuderi Drago et al. 2001). The microwave opacity in filaments is provided by free-free emission in the ionized component. Prominences above the limb will also appear in emission if they are dense enough (Kundu 1972; Hanaoka et al. 1994; Gopalswamy et al. 1996, 1997; Gopalswamy & Hanaoka 1998; Gopalswamy et al. 2003). In this event the filament is clearly seen as a stationary depression prior to its gradual rise, and we can follow its evolution in the radio images. Figure 2 presents radio contours chosen to show the filament location, overlaid on the available EIT 195 Å images to show the coincidence in position at radio and EUV wavelengths. The temperature depression of the radio feature against the disk is typically 3000 – 5000 K, as expected, but once the material can be seen above the limb it is seen as an emission feature with a brightness temperature of 9000 – 12000 K. At 04:50 UT the filament is seen simultaneously both as a depression just inside the limb and an emission feature just above

the limb.

NoRH data are available at a cadence as short as 1 second. To track the motion of the filament we have made maps during the gradual rise at 1 minute intervals and measured the position of the filament relative to its initial position using the location of the minimum in the depression averaged over the central portion of the filament while it is on the disk, and the leading edge of the filament material once it is seen in projection above the limb. The resulting measurements are shown in Figure 3. The noise level in the height measurements may be estimated from the point-to-point variations. Once it starts moving at about 03:35 UT, there seem to be three stages in the filament motion: a gradual rise with roughly constant acceleration until about 04:45 UT, a phase of very rapid acceleration between 04:45 and 04:55 UT, and a period of constant velocity, or at least slower acceleration, after 04:55 UT. After 05:00 UT the legs of the filament are still visible in the radio images, but the leading edge is no longer discernible above the background. From a movie of the images, the evolution appears to be the well-known pattern of accelerating stretching of a loop-like structure in which the legs stretch outwards relatively slowly but the apex of the loop accelerates much more rapidly.

Between 03:35 and 04:45 UT the acceleration of the bulk of the filament is probably not constant but rather increasing gradually: the figure shows a fiducial line corresponding to a constant acceleration of 15.4 m s^{-2} which is initially faster than the observed acceleration. A dashed line shows a constant velocity of 425 km s^{-1} for comparison with the height measurements after 04:50 UT; the separation of the last two points on the plot corresponds to a velocity of 650 km s^{-1} , which is closer to the speed we will infer below from the LASCO data. Prior to 05:00 the filamentary material visible in the radio images seems to be well characterized by a common velocity, but at times after 05:00 this is not the case because both the radio and the LASCO images indicate that the outer edge of the filament is travelling much faster than the legs of the filament once it stretches to heights above about $1 R_{\odot}$.

The period of rapid acceleration between 04:45 and 04:50 UT roughly coincides with the transition of the filament from projection against the disk to projection above the limb. The filament lifted off from about E45, and we assume it to travel roughly radially, implying that the projected distances are a factor of 1.4 smaller than the true distances travelled. We argue that the occurrence of the rapid acceleration phase when the filament reaches the limb in projection is purely coincidence: it only appears this way from our viewpoint and would not be the case from any other viewing direction. In fact, the last few measurements inside the limb indicate that the rapid acceleration phase has already commenced. We argue below that the rapid acceleration coincides with another feature of the event, namely the impulsive phase of the associated flare. The apparent filament speed, i.e. projected onto the sky plane, at around 04:45 UT is 50 km s^{-1} ; by 05:00 UT, the speed may already be as high as 650 km s^{-1} , which is faster than any of the sample of 174

erupting prominences studied by Gopalswamy et al. (2003). Hanaoka & Shinkawa (1999) report an erupting filament that they could track over large distances across the solar disk because it obscured bright active regions at 17 GHz as it passed in front of them. Projected velocities for the filament in that event are of order $300 - 470 \text{ km s}^{-1}$. Wang et al. (2003) report EIT observations of filamentary material travelling at a deprojected speed of 580 km s^{-1} , while Gopalswamy et al. (2003) note that CME cores observed by LASCO have peak speeds in the range $600 - 800 \text{ km s}^{-1}$ at heights corresponding to the LASCO C2 field of view (their Fig. 14).

While the overall pattern of filament motion is clear from Fig. 3, there is sufficient noise in the measurements, complicated by the transition from an absorption to an emission feature, to make it difficult to derive a detailed acceleration profile. The second derivative of a smoothed version of Fig. 3 shows a peak between 04:45 and 04:50. The average acceleration between 04:45 (velocity 50 km s^{-1}) and 04:54 (assuming 425 km s^{-1}) is 700 m s^{-2} . By comparison, Gilbert et al. (2000) found only one out of 17 erupting prominences in their H α study with an acceleration in excess of 100 m s^{-2} . The value of 700 m s^{-2} is also larger than is found in most CMEs, which is more typically a few hundred m s^{-2} (Zhang et al. 2001; Neupert et al. 2001), although Zhang et al. (2001) report acceleration of 7300 m s^{-2} in a CME associated with an X9 flare.

3. SOFT X-RAY OBSERVATIONS OF THE RISING FILAMENT

This event was observed by the Soft X-ray Imager (SXI) on the GOES 12 satellite. A sequence of images during the filament’s gradual rise phase is shown in Figure 4. The first sign of activity associated with the filament’s rise is a brightening due north of the active region, seen at coordinates $-640''$, $-100''$ (relative to disk center) in the image at 04:09 UT (labelled). This feature continues to brighten, and develops an extension to the southwest. At 04:17 UT a new feature is visible: a faint long loop-shaped feature extending from the active region in the south about $300''$ northwards, curving around the initial brightening. This feature is also visible in EIT 195 Å images. Difference images show that the largest increase in emission associated with this loop occurs at its southern end, close to the original location of the visible filament. The sequence of SXI images shows this loop feature moving outwards in the same direction as the filament. The north and south ends of the loop appear to be anchored while the central portion moves eastwards and fades by 04:30 UT. The motion can be seen in Fig. 4 between 04:17 and 04:24 (the lines in the two panels are in the same location). Difference images also show a dimming in the location marked at 04:31, to the north of the original soft X-ray brightening and underneath the long loop. The subsequent flare loop, shown in the image at 05:16 UT, is in the active region to the south.

If we compare 195 Å, radio and SXI images at the same time, we find that the radio and 195 Å depressions corresponding to the moving filament coincide, while the long soft X-ray loop lies

to the west, or underneath, the dark filament. This suggests energy release on long field lines in the region underneath the filament, disturbed by the passage of the filament material.

4. THE CORONAL MASS EJECTION

A halo CME was reported by the Large Angle Spectroscopic Coronagraph (LASCO) on the SOHO satellite in conjunction with this event. Unfortunately no LASCO images are available between 04:30 and 05:30 UT; the first image showing the CME is at 05:30 UT, when it has already reached a projected height of $3.8 R_{\odot}$ above the solar limb (Figure 5). The analysis of the LASCO data (see the CDAW CME catalog at http://cdaw.gsfc.nasa.gov/CME_list/) indicates a mean CME speed of 1380 km s^{-1} . At this mean speed, the launch time of the CME at the solar surface would be between 04:50 and 05:00 UT.

The bulk of the CME comes out to the east, consistent with the original location of the filament. The filament we are following is clearly visible close to the equatorial plane, with a stretched appearance suggesting that the southern leg of the filament is travelling much slower than the outer edge, as seen in the radio images. The leading edge of the filament is at a projected height of about $2.4 R_{\odot}$ above the solar limb at 05:30 UT.

However, the coronagraph image suggests that the event was not simple: the outer edge of the CME consists of two arcs, with one centered south of the equator and the other north of the equator, and both arcs appear to have filamentary material in their cores. Careful inspection of $H\alpha$ images spanning the event (available from the New Jersey Institute of Technology Big Bear Solar Observatory archive at <ftp://ftp.bbso.njit.edu/pub/archive/2001/11/17/>) shows that no filament on the front (visible) side of the northern hemisphere vanished during the relevant time period, suggesting the possibility that the northern event is due to a filament eruption behind the limb in the northern hemisphere. However, the NoRH 34 GHz images clearly indicate that the northern filament is an extension of the southern filament and originates on the visible disk, and is either the northern part of the filament visible in Figure 1 or else is not visible in $H\alpha$ images prior to the flare.

Comparing the C2 images at 05:30 and 05:54, we measure a propagation speed of 820 km/s for the northern filamentary arc. It is more difficult to measure a speed for the southern filamentary arc which is more diffuse than the northern arc, but its outer edge appears to have a speed of order 700 km s^{-1} in this interval. The LASCO C2 image at 05:54 UT also suggests that the northern and southern filaments are connected, but projection effects confuse the situation. The fact that only one filament erupted makes the bilobate shape of the outer envelope of the CME at 05:30 UT somewhat puzzling. The two lobes of the CME appear to have different speeds: by comparing the

locations of the outer envelopes of the northern and southern lobes in the LASCO C3 images at 05:43 and 06:19 UT, we measure a speed of 1440 km s^{-1} for the northern lobe but $1200 \pm 100 \text{ km s}^{-1}$ for the southern lobe (the uncertainty is larger for the southern lobe because its outer edge is more diffuse than the northern lobe’s).

Concentrating on the southern lobe of the CME and the southern section of the filament, whose motion is shown in Fig. 3, at the projected time of the CME liftoff (04:50 UT) the filament has already reached a height of $2 \times 10^{10} \text{ cm}$ above its original location. If the filament continues to move outwards at 650 km/s , it would reach a height of $2.4 R_{\odot}$ above the limb at 05:30 UT. The LASCO image at 05:30 UT shows the outermost filamentary material to be at about this height, while the leading edge of the CME is at a height of $3.8 R_{\odot}$. In the normal CME scenario the bulk of the material that makes up the CME would come from heights above the associated filament: if that scenario were true here, then the CME material is originally located above a deprojected height of order $3 \times 10^{10} \text{ cm}$. Since the density at these heights is low, it is more likely that the CME material also originates at lower heights and so also has a slower acceleration period prior to the impulsive phase of the flare. Extrapolating the CME backwards from $3.8 R_{\odot}$ at 1200 km/s , its height intersects that of the filament at about 04:55–05:00 UT, consistent with the idea that the CME undergoes rapid acceleration at the same time as the filament.

5. THE FLARE

In addition to the filament eruption and the CME, this event features a long and complex GOES class M2.8 flare originating in NOAA active region 9704 (S18E41), to the south and west of the original filament location and south of the initial soft X-ray brightening seen in the SXI images (Fig. 4). The brightest flare loop is in the active region, as shown by the SXI image at 05:16 UT in Fig. 4. Figure 6 shows radio light curves for the flare at several frequencies, together with a prediction of the radio flux expected due to thermal bremsstrahlung from the soft X-ray emitting plasma detected by GOES. The 3.75 GHz light curve shows a clear impulsive phase starting at 04:45 UT and peaking at 05:00 UT. From the absence of this peak in the higher frequency light curves, we infer that this is due to gyrosynchrotron emission from nonthermal electrons. The higher frequencies of 17 and 34 GHz both show more gradual light curves in the total flux; the images at these frequencies at later times are dominated by emission from large-scale post-flare loops (see below) and thus the light curves represent thermal bremsstrahlung from these loops. They would be expected to resemble the GOES-predicted thermal bremsstrahlung radio flux, as they do.

A Type II radio burst was reported to be present between 145 and 45 MHz from 04:50 to 04:55 by Learmonth Observatory, and can be seen in the Bruny Island Radio Spectrometer (BIRS)

data below 50 MHz as a very brief fundamental–harmonic Type II burst lasting only from 05:01 to \sim 05:05. The presence of the Type II burst in this time period is consistent with an impulsive phase at around 04:45–04:50 UT. We note that the Type II burst is not observed until after the filament undergoes its rapid acceleration phase.

Radio images of the flare at 17 and 34 GHz from NoRH data are shown in Figure 7. The brightest feature in the active region at 17 GHz both before and during the flare is a double source lying over a sunspot (coordinates $-580''$, $-340''$), with a brightness temperature prior to the flare in excess of 10^5 K. This is likely to be a thermal coronal gyroresonance source in the strong magnetic field of the sunspot, since it is not present at 34 GHz. At 04:50, during the rise of the impulsive phase of the flare, the brightening to the north of the active region, visible earlier in the SXI images (Fig. 4), has continued to brighten (it is present as a single small contour at 04:30 UT at coordinates $-680''$, $-120''$, underneath the original location of the filament). Simultaneously the source over the northern sunspot (coordinates $-580''$, $-320''$) starts to brighten, and a linear feature stretching from this sunspot towards the north–east appears. By 04:55 another linear feature to the south has brightened and linked up with the northern linear feature to form a loop–shaped structure to the north–east of the sunspot source and connected to the northern component of it at 17 GHz. This loop–shaped structure (peaking at coordinates $-650''$, $-250''$) dominates the 34 GHz image from 04:55 UT onwards. While this source looks like a loop, in fact the uneven brightness distribution indicates that it is composed of several segments. It also dominates the SXI soft X–ray image (Fig. 4) and the EIT Fe XII 195 Å image (last panel of Fig. 7).

The radio spectrum from 17 to 34 GHz for this loop feature is consistent with a constant flux versus frequency, indicating that the emission is thermal bremsstrahlung. However the emission from the sunspot source at coordinate $-580''$, $-320''$, whose flux increases by about a factor of 5 during the flare, is nonthermal. In fact its emission has a profile quite different from the smooth thermal component evident in the overall 17 and 34 GHz light curves (Fig. 6), but is quite similar to that of the 3.75 GHz light curve. We therefore argue that the nonthermal microwave emission in the impulsive phase of this event originates close to the sunspots in the active region. The 34 GHz images also show a weak source spatially coincident with the northern component (but not the southern component) of the 17 GHz sunspot source from about 05:00 to 05:15 UT (greyscale images in Fig. 7).

As the flare develops, the flare radio and soft X–ray emission spread to the north and north–east of the brightest soft X–ray loop, reaching the original location of the filament by 05:30 UT (Fig. 7). This confirms the association between the flare, CME and filament eruption despite the considerable distance between the original filament location and the active region where the main flare occurs.

6. DISCUSSION

6.1. Motion of the erupting filament

We have studied a gradual filament eruption associated with a GOES class M2.8 solar flare and a fast CME using a wide range of data sources. Studies such as this are excellent examples of the power of having multiple data sets (in this case, NoRH, NoRP, EIT, LASCO, MDI, SXI, GOES, BBS, GMRT and SOON) freely accessible. The event commences with the gradual rise of a filament lying over a quiet region of the Sun's surface at around 03:40 UT, proceeding with approximately constant acceleration until the impulsive phase of the associated flare at around 04:45 UT. The flare takes place in an active region $100''$ from the filament's original location: by the time the flare starts, the filament is almost $300''$ away (in projection).

Since this is the same time that the rapid acceleration of the erupting filament is observed by NoRH, changing velocity from 50 km s^{-1} to $\sim 650 \text{ km s}^{-1}$, we argue that this event is strikingly similar to the scenario for CME acceleration presented by Zhang et al. (2001) and Neupert et al. (2001). Using EIT and LASCO data for CMEs visible in the field of view of the LASCO C1 camera to study their onset, Zhang et al. (2001) argued that there are three phases to the eruption: (i) initiation, characterized by a slow ascension with a speed less than 80 km s^{-1} for tens of minutes prior to the impulsive phase; (ii) impulsive acceleration, in which the CME undergoes dramatic acceleration coincident with the rise phase of the associated flare; and (iii) propagation, characterized by constant or slowly changing CME speed. In their data, the acceleration of the CME ceases near the peak time of the flare soft X-ray emission, to within the limited cadence of the LASCO images. The acceleration rates in the impulsive acceleration phase are typically in the range of $100\text{-}500 \text{ m s}^{-2}$.

The observations of the filament reported here follow the pattern identified for CMEs very closely and suggest that the acceleration at the impulsive phase of the associated flare applies to all the erupting material. Each of the three phases described by Zhang et al. (2001) is exhibited by the erupting filament in this event (Fig.3). This event is slightly anomalous in that the filament has reached a (deprojected) height of almost half a solar radius before the flare and the rapid acceleration take place, but it still fits the pattern that the filament is much slower than the CME, both low in the atmosphere as an erupting filament, and high in the atmosphere as the CME core which typically has half the CME speed (Gopalswamy et al. 2003, Figure 14). Note however that the prime data source for the study of the eruption here is not coronagraph or EUV data, but radio observations that strikingly show the filament as a depression against the solar disk and then as an emission feature above the solar limb.

Zhang et al. (2001) find that the rapid acceleration phase for CMEs ceases near the peak time of the soft X-ray emission (actually, of the $1\text{-}8 \text{ \AA}$ channel of the GOES soft X-ray detectors).

In this event the rapid phase of filament acceleration ceases by 05:00 UT, well before the 1–8 Å GOES peak which is at around 05:30 UT (although we note that the 0.5–4 Å GOES channel peaks earlier at about 05:10 UT). This difference in the duration of the rapid acceleration phase in this filament eruption compared to the CMEs studied by Zhang et al. (2001) may be real, but we note that the EIT and LASCO data available to Zhang et al. (2001) and Neupert et al. (2001) had a cadence of no better than about 10 minutes, so they could not investigate the relationship between the flare impulsive phase and CME acceleration on finer timescales. In at least two of the four events studied by Zhang et al. (2001, 1998 Jun 11 and 1997 Feb 23), and in one of the three events studied by Neupert et al. (2001, 1998 May 8 at 13 UT; in the event on the same day at 2 UT acceleration must continue well after the soft X-ray peak), the data could also be consistent with acceleration ending significantly before the 1–8 Å soft X-ray peak. Since Zhang et al. (2001) themselves are careful to note that their data only indicate that CME acceleration “stops at a time close to the peak time of the X-ray flux”, we do not presently regard this discrepancy as significant.

6.2. Comparison with a magnetic flux rope model

Chen & Krall (2003) have studied the acceleration of coronal mass ejections and erupting filaments in the context of a three-dimensional flux rope model for these phenomena (Chen 1989, 1996). In this model the flux rope consists of a shell of current density with both poloidal and toroidal components, generating a rope of helical magnetic field lines surrounded by an ambient field. The current circuit closes through the photosphere. The eruption is driven by the injection of poloidal magnetic flux into the rope from the photosphere, changing the Lorentz self-forces between the current system and its magnetic field. This model naturally reproduces the three-phase pattern of acceleration described above. The maximum acceleration of the flux rope is attained shortly after the height of the apex of the flux rope exceeds a critical height at which the radius of curvature of the rope is minimized. For fixed footpoints, this critical height is half the footpoint separation. Acceleration is essentially complete by the time the flux rope reaches three times the critical height.

Due to the nature of coronagraphs, it will always be difficult to determine the location of the footpoints of a CME; it is observationally easier to test the predictions of this model for an erupting filament which can be seen in the lower atmosphere, and we can investigate whether whether the flux rope relationship holds for this event. Since the external forces on the flux rope are generally smaller than the self-forces, unlike other models for CMEs such as the tether-cutting (Sturrock 1989; Moore et al. 1997, 2001) and the breakout (Antiochos et al. 1999; Aulanier et al. 2000; Sterling & Moore 2001) models where external conditions are more important, the flux rope model applies equally well to an erupting filament and a coronal mass ejection.

The location of the northern footpoint of the erupting filament is quite clear from the SXI and the EIT 195 Å images: it lies at the northern end of the long loop observed by SXI in conjunction with the slow acceleration phase of the filament’s rise (e.g., Fig. 4, 04:24 UT), at about coordinate $-610''$, $+100''$. The location of the southern footpoint is not as clear from the images, but it appears to be close to the southern end of the SXI loop at coordinate $-770''$, $-260''$, just south of the original location of the H α filament. The linear dimension of this feature is about $390''$ in a predominantly north–south orientation, and therefore it does not suffer from projection effects. This implies a critical height for the filament of order 1.4×10^5 km. At 04:45 when the filament’s acceleration is observed to peak, it has a (deprojected) height of 1.8×10^5 km, assuming that it rises radially upwards. The filament reached the critical height at about 4:37 UT, but remained in a state of slow acceleration for at least another 5 minutes. For the acceleration profile of the filament to peak at the critical height, the footpoint separation would need to be $500''$, which we believe is not supported by the observations since even if the southern footpoint of the filament lies in AR 9704 the footpoint separation is still only $400''$. However, these measurements could still be consistent with the Chen & Krall (2003) model since the authors point out that the exact height at which maximum acceleration occurs depends somewhat on the detailed structure of the filament current profile, with the only firm constraint being that it will occur above the critical height as we find here.

6.3. Relationship between filament acceleration and flare

The coincidence of the impulsive phase of the flare and the rapid acceleration phase of the filament despite the large spatial separation of the two events is the most striking feature of this study. There has to be a trigger that causes the rapid acceleration of the erupting filament to occur at the same time as the impulsive phase of the flare (just as, in the scenario presented by Zhang et al. 2001, a trigger is needed to cause the rapid acceleration of CMEs at the same time as the flare impulsive phase). We argue that the impulsive phase of the flare occurs in the low corona in AR 9704, because (a) the brightest soft X–ray emission takes place just to the north–east of the sunspot in this region, at coordinate $-650''$, $-250''$; (b) the NoRH 17 GHz images show that the nonthermal radio emission at 17 GHz is located close to the sunspot at $-680''$, $-320''$, and the light curve of this source is very similar to the 3.75 GHz light curve that has a nonthermal spectrum and so, by inference, probably comes from a similar location. At the time of the maximum acceleration at 04:45 UT, the filament is at least 1.8×10^5 km away from the flare location.

Two types of mechanism can be envisaged for the trigger: a disturbance that propagates from one site to the other at high speed; or a large scale event that causes both phenomena to happen together. At a typical coronal Alfvén speed of 500 km s^{-1} , the time taken by a disturbance to

propagate from one location to the other would be over 5 minutes. In this event it seems unlikely that any disturbance would propagate from the filament back to the active region to cause the flare there. The old view used to be that the flare blast caused any associated CME but in this case, apart from the observation of a Type II burst, there is little evidence for the impulsive type of blast usually envisaged in this scenario since all the other flare diagnostics change relatively gradually from 04:45 to 05:00 UT, and the filament is so far from the flare site at 04:45 that it seems unlikely to be affected directly by a blast wave from the flare.

As also argued by Zhang et al. (2001) for CMEs, a large-scale disruption of the magnetic field, such as occurs in the tether-cutting and breakout models, is the type of trigger that seems to fit the pattern observed: it could release energy in the active region at the same time as it removes the impediments restraining the acceleration of the filament. In the flux rope model of Chen & Krall (2003) one can readily imagine flares occurring at one of the footpoints of the flux rope where magnetic flux is being injected and the coronal magnetic field is being disturbed. It is more difficult to see how a flare could occur in this model well away from the footpoints of the erupting flux rope, as seems to be the case here, since the magnetic field at such a remote location would not be expected to be disturbed by any self-contained flux rope changes. A flare at a remote location could occur if field lines rooted there are disrupted by the eruption of the flux rope, but this implies that field lines external to the flux rope play a significant role in inhibiting the eruption (in order to explain the simultaneity of the flare and the rapid acceleration phase), and in that case the model's universal scaling law that depends predominantly on the parameters of the flux rope alone (i.e., the footpoint separation) would not seem to apply.

7. CONCLUSIONS

We have used radio imaging data from the Nobeyama Radio Heliograph in conjunction with data from a wide range of other sources to study an erupting filament event associated with a fast CME and a flare. The advantage of the radio data is the high cadence they possess, permitting us to follow the motion of the filament at high spatial resolution and high time resolution. The radio data are also able to fill in gaps in the EIT and LASCO coverage of the impulsive phase of the event.

The striking feature of the eruption is the rapid acceleration of the filament at the time of the impulsive phase of the associated flare, following a very long period of gradual acceleration that led to soft X-ray and EUV emission under the rising filament but little other trace of energy release. Once the rapid acceleration has occurred, the apex of the filament propagates outwards at high speed, with lesser or no acceleration, while the legs of the filament stretch out below it. The height-time profile of the CME is consistent with rapid acceleration at the same time as the filament, since a different behaviour would lead to the CME material originating at heights

underneath the filament. This event shows the same three phases of acceleration that Zhang et al. (2001) and Neupert et al. (2001) report for flare-associated CMEs: gradual acceleration prior to the impulsive phase of the flare, then very rapid acceleration during the impulsive phase and slower or no acceleration thereafter. The flare in this event seems to occur well away from the footpoint of the erupting filament, which favors a model in which a large-scale disruption of the coronal magnetic field takes place, permitting the simultaneous launch of the filament/mass ejection and the release of energy in the flare site. The flare site and the filament are so far apart at the time of the impulsive phase that a disturbance propagating from one site to the other to trigger the simultaneous events seems very unlikely.

At the University of Maryland this research was supported by NSF grant ATM 99-90809 and NASA grants NAG 5-11872, NAG 5-12860 and NAG 5-10175. We thank those responsible for NoRH, NoRP, EIT, LASCO, MDI, BBSO and SXI for making their data readily available for scientific use. SXI is operated by NOAA. We thank an anonymous referee for pointing out an error in the interpretation of the LASCO data, and a second referee for careful comments that led to improvements in the manuscript.

REFERENCES

- Antiochos, S. K., Devore, C. R., & Klimchuk, J. A. 1999, *Astrophys. J.*, 510, 485
- Aulanier, G., DeLuca, E. E., Antiochos, S. K., McMullen, R. A., & Golub, L. 2000, *Astrophys. J.*, 540, 1126
- Chen, J. 1989, *Astrophys. J.*, 338, 453
- . 1996, *J. Geophys. Res.*, 101, A12, 27499
- Chen, J. & Krall, J. 2003, *J. Geophys. Res.*, 108, A11, 1410
- Chiuderi Drago, F. 1990, in *IAU Colloq. 117: Dynamics of Quiescent Prominences* (Berlin: Springer-Verlag), 70–83
- Chiuderi Drago, F., Alissandrakis, C. E., Bastian, T., Bocchialini, K., & Harrison, R. A. 2001, *Solar Phys.*, 199, 115
- Chiuderi-Drago, F., Furst, E., Hirth, W., & Lantos, P. 1975, *Astron. Astrophys.*, 39, 429
- Drago, F. C. & Felli, M. 1970, *Solar Phys.*, 14, 171
- Gilbert, H. R., Holzer, T. E., Burkepile, J. T., & Hundhausen, A. J. 2000, *Astrophys. J.*, 537, 503
- Gopalswamy, N. & Hanaoka, Y. 1998, *Astrophys. J. (Lett.)*, 498, L179
- Gopalswamy, N., Hanaoka, Y., Kundu, M. R., Enome, S., Lemen, J. R., Akioka, M., & Lara, A. 1997, *Astrophys. J.*, 475, 348
- Gopalswamy, N., Kundu, M. R., Hanaoka, Y., Enome, S., Lemen, J. R., & Akioka, M. 1996, *New Astronomy*, 1, 207
- Gopalswamy, N., Shimojo, M., Lu, W., Yashiro, S., Shibasaki, K., & Howard, R. A. 2003, *Astrophys. J.*, 586, 562
- Hanaoka, Y., Kurokawa, H., Enome, S., Nakajima, H., Shibasaki, K., Nishio, M., Takano, T., Torii, C., Sekiguchi, H., Kawashima, S., Bushimata, T., Shinohara, N., Irimajiri, Y., Koshiishi, H., Shiomi, Y., Nakai, Y., Funakoshi, Y., Kitai, R., Ishiura, K., & Kimura, G. 1994, *Publ. Astron. Soc. Japan*, 46, 205
- Hanaoka, Y. & Shinkawa, T. 1999, *Astrophys. J.*, 510, 466
- Illing, R. M. E. & Hundhausen, A. J. 1986, *J. Geophys. Res.*, 91, 10951

- Kahler, S. W., Moore, R. L., Kane, S. R., & Zirin, H. 1988, *Astrophys. J.*, 328, 824
- Kundu, M. R. 1970, *Solar Phys.*, 13, 348
- . 1972, *Solar Phys.*, 25, 108
- Moore, R. L., Schmieder, B., Hathaway, D. H., & Tarbell, T. D. 1997, *Solar Phys.*, 176, 153
- Moore, R. L., Sterling, A. C., Hudson, H. S., & Lemen, J. R. 2001, *Astrophys. J.*, 552, 833
- Munro, R. H., Gosling, J. T., Hildner, E., MacQueen, R. M., Poland, A. I., & Ross, C. L. 1979, *Solar Phys.*, 61, 201
- Neupert, W. M., Thompson, B. J., Gurman, J. B., & Plunkett, S. P. 2001, *J. Geophys. Res.*, 106, 25215
- Sterling, A. C. & Moore, R. L. 2001, *J. Geophys. Res.*, 106, 25227
- Sturrock, P. A. 1989, *Solar Phys.*, 121, 387
- Subramanian, P., Ananthkrishnan, S., Janardhan, P., Kundu, M. R., White, S. M., & Garaimov, V. I. 2003, *Solar Phys.*, in press
- Wang, H. & Goode, P. R. 1998, in *ASP Conf. Ser. 140: Synoptic Solar Physics*, ed. J. H. K. S. Balasubramanian & D. Rabin (San Francisco: Astron. Soc. Pacific), 497
- Wang, H., Qiu, J., Jing, J., & Zhang, H. 2003, *Astrophys. J.*, 593, 564
- Webb, D. F., Krieger, A. S., & Rust, D. M. 1976, *Solar Phys.*, 48, 159
- Zhang, J., Dere, K. P., Howard, R. A., Kundu, M. R., & White, S. M. 2001, *Astrophys. J.*, 559, 452

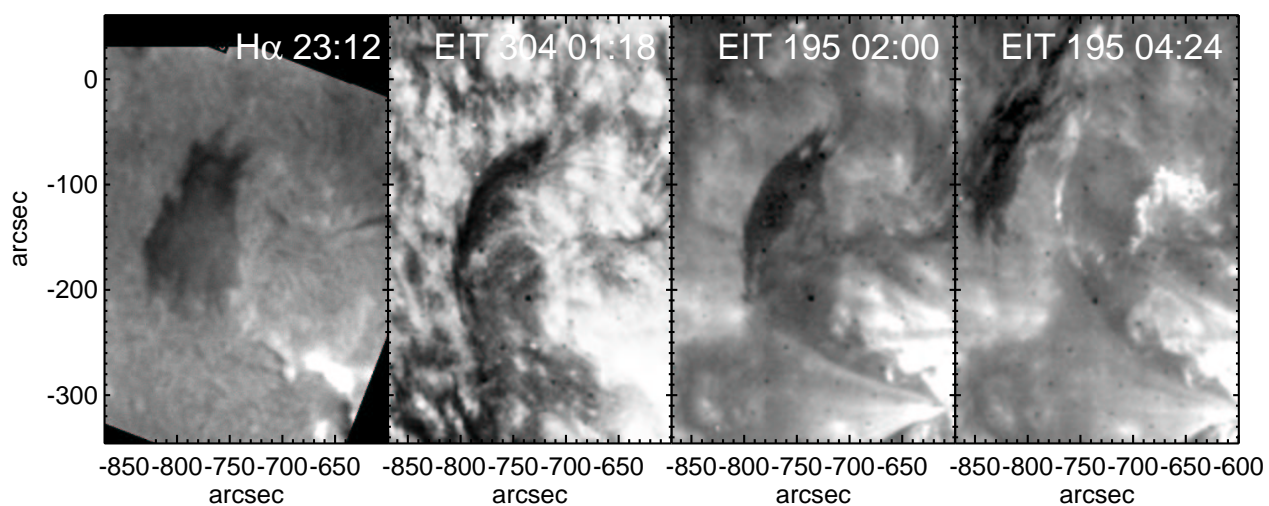


Fig. 1.— Images of the filament prior to eruption in $H\alpha$ at 23:12 UT on November 16 (Holloman Air Force Base image), in He 304 Å at 01:18 UT on November 17 (SOHO/EIT image), and in Fe XII 195 Å at 02:00 and 04:24 UT (SOHO/EIT images). AR 9704 is visible in the lower right corner of each panel. The slow rise of the filament is evident in the difference in positions between the 02:00 and 04:24 EIT images: the first clear sign of motion in the EIT image sequence is at 03:48 UT.

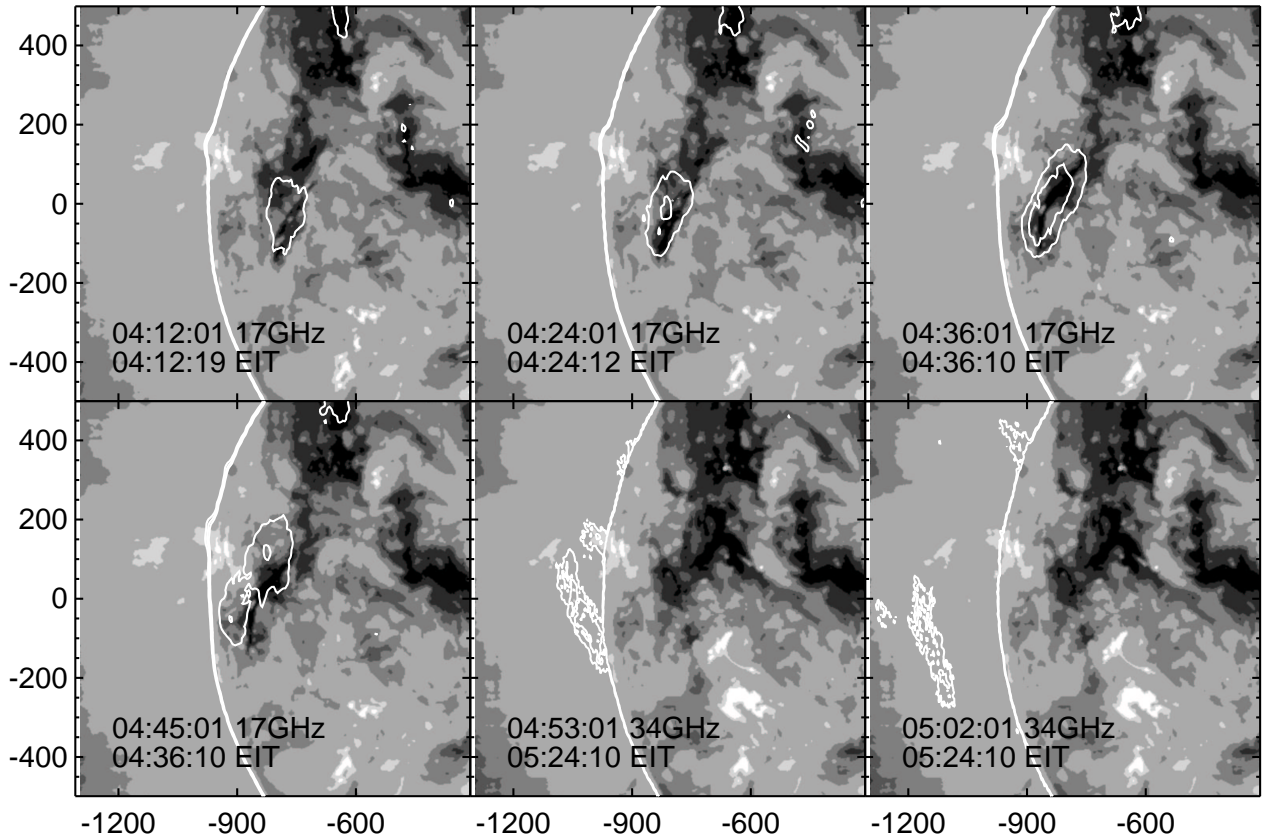


Fig. 2.— Overlays of contours of the NoRH radio images on the EIT 195 Å images demonstrating the motion of the filament against the disk and its continuation in the radio images above the limb. The erupting filament is seen as a dark feature in the EIT images until the last EIT image, at 04:24, before the data gap. The first 4 radio images, in which the filament is seen as a depression of radio emission in projection against the bright disk, are 17 GHz images while the last two radio images are at 34 GHz, where the material above the limb emits with a brightness temperature of order 9000 – 12000 K above the dark background.

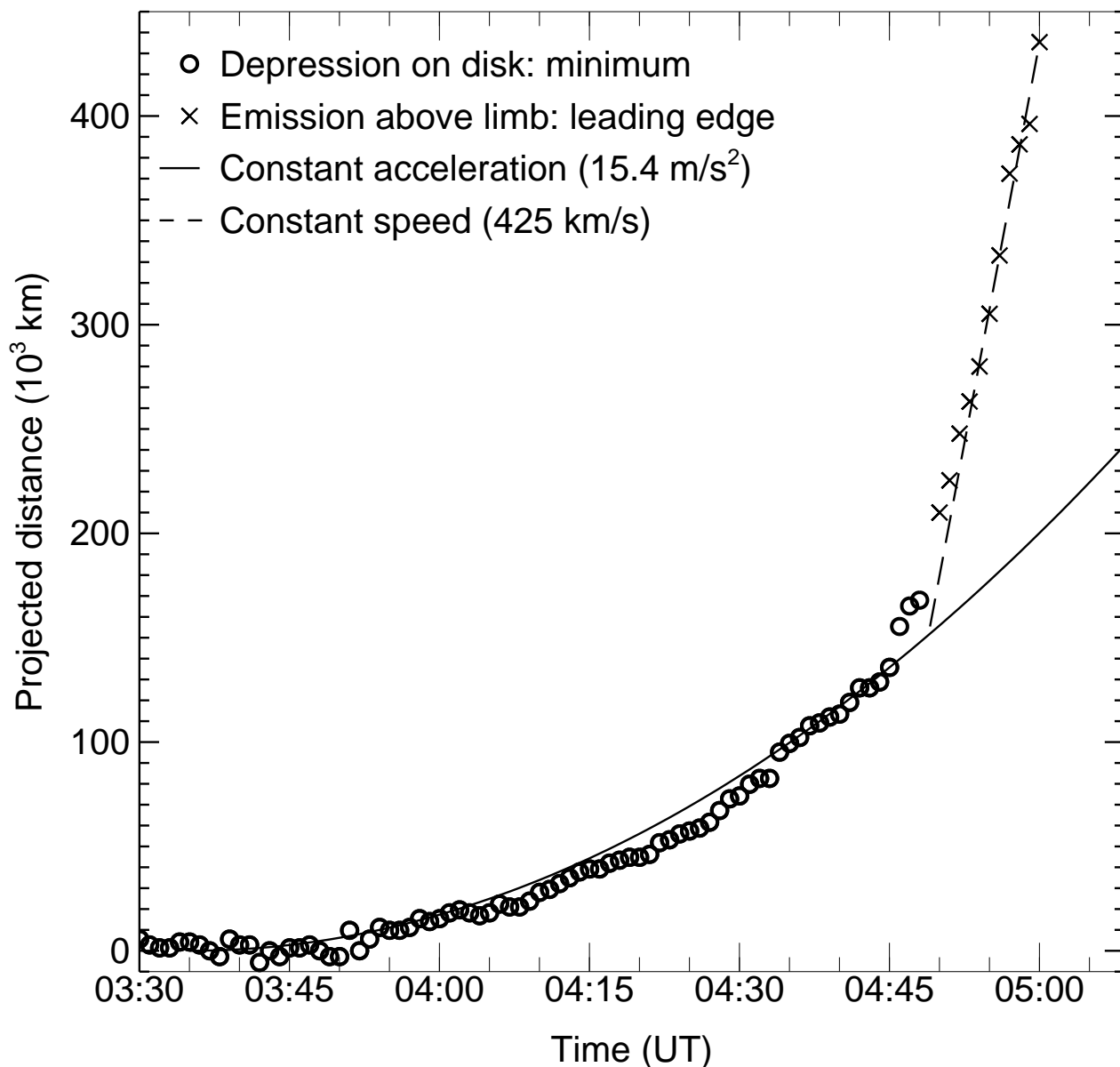


Fig. 3.— The motion of the erupting filament from NoRH 34 GHz data. The circles show the position of the depression minimum while the filament was seen against the solar disk, averaged over $100''$ vertically after rotating the images 22° anticlockwise to bring the filament motion to the horizontal direction. The filament was typically 4000 K below the disk brightness temperature. The crosses show the location of the leading edge once the filament became visible as an emission feature above the limb. For comparison, we have plotted a (solid) line of constant acceleration (15 m s^{-2}) that loosely fits the circles, and a (dashed) line of constant velocity (425 km s^{-1}) for comparison with the measured heights above the limb: the outer edge of the filament appears to accelerate rapidly between 04:45 and 04:55 UT. The distances shown are those measured in projection on the sky: if the filament is moving radially outwards from about E45 on the solar disk, the true distances are larger by about a factor of 1.4.

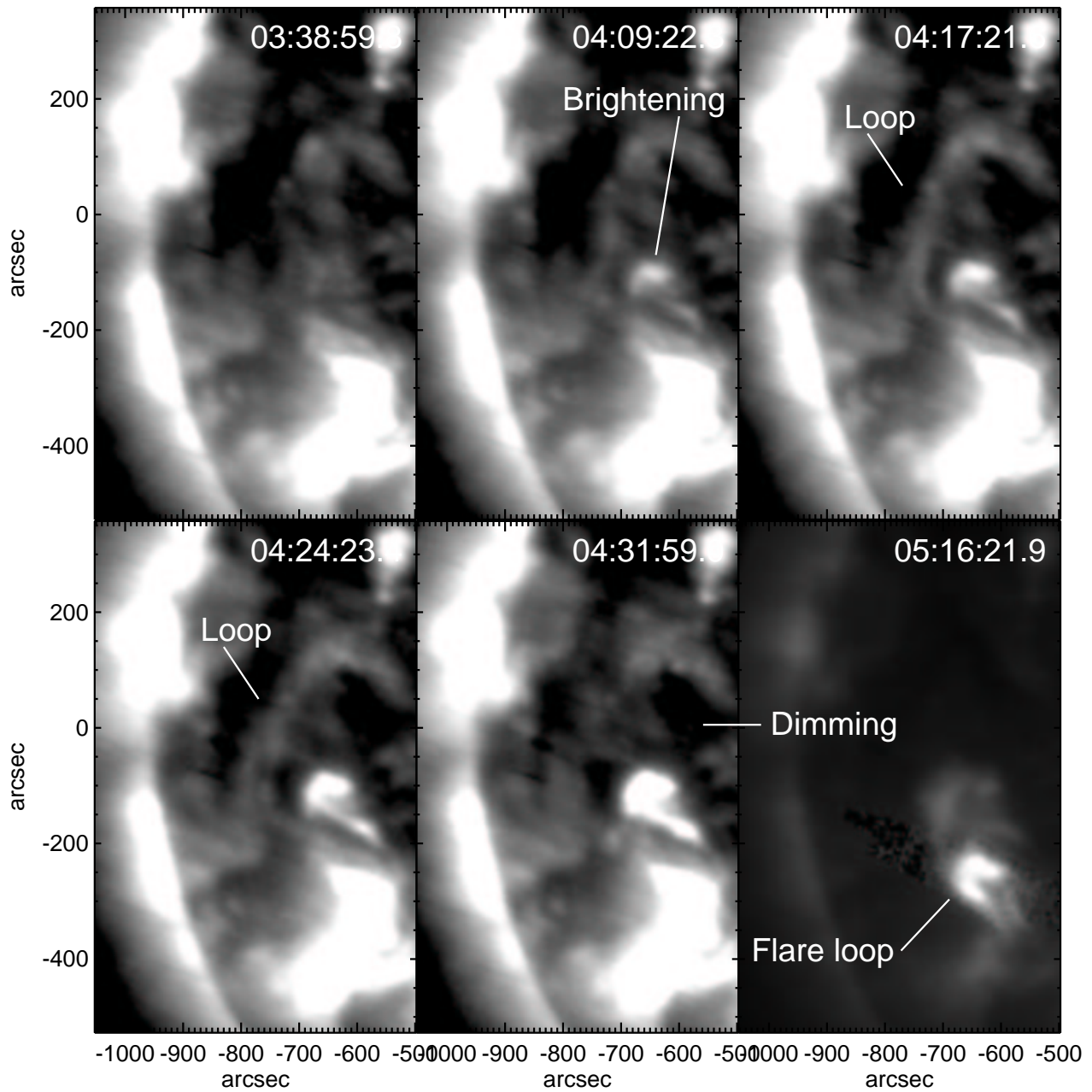


Fig. 4.— A sequence of SXI images acquired with the open filter. The images are long (3 s) exposure, with saturated pixels replaced by the corresponding unsaturated pixels from the subsequent short exposure taken typically 1 minute later. In the first 5 images the color table is chosen to emphasize weak features: the long soft X-ray loop associated with the erupting filament is indicated in the third and fourth frames, and its motion can be seen. The last frame shows the soft X-ray morphology much later, near the peak of the flare soft X-ray emission.

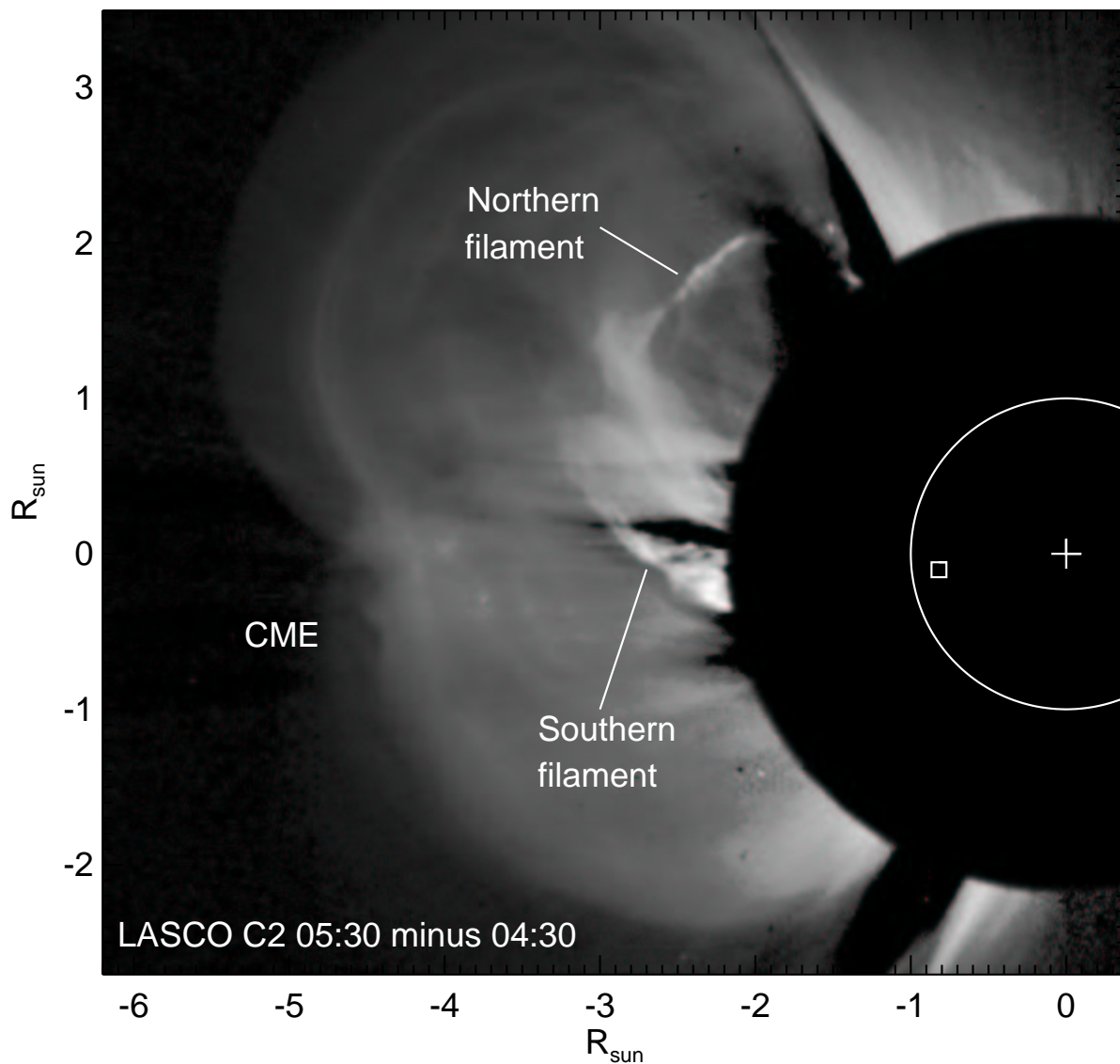


Fig. 5.— SOHO/LASCO C2 coronagraph difference image (05:30 UT minus 04:30 UT) of the CME on 2001 November 17. This is the first available LASCO image of the CME due to a gap in coverage between 04:30 and 05:30. The solar limb is marked by a circle, disk center by a plus symbol, and the location of the filament prior to eruption by a square. The sections of filament south and north of the equator are labelled, as is the leading edge of the CME, which can be seen to be bilobate, i.e., consisting of two arcs, one in the southern hemisphere and the other in the northern hemisphere.

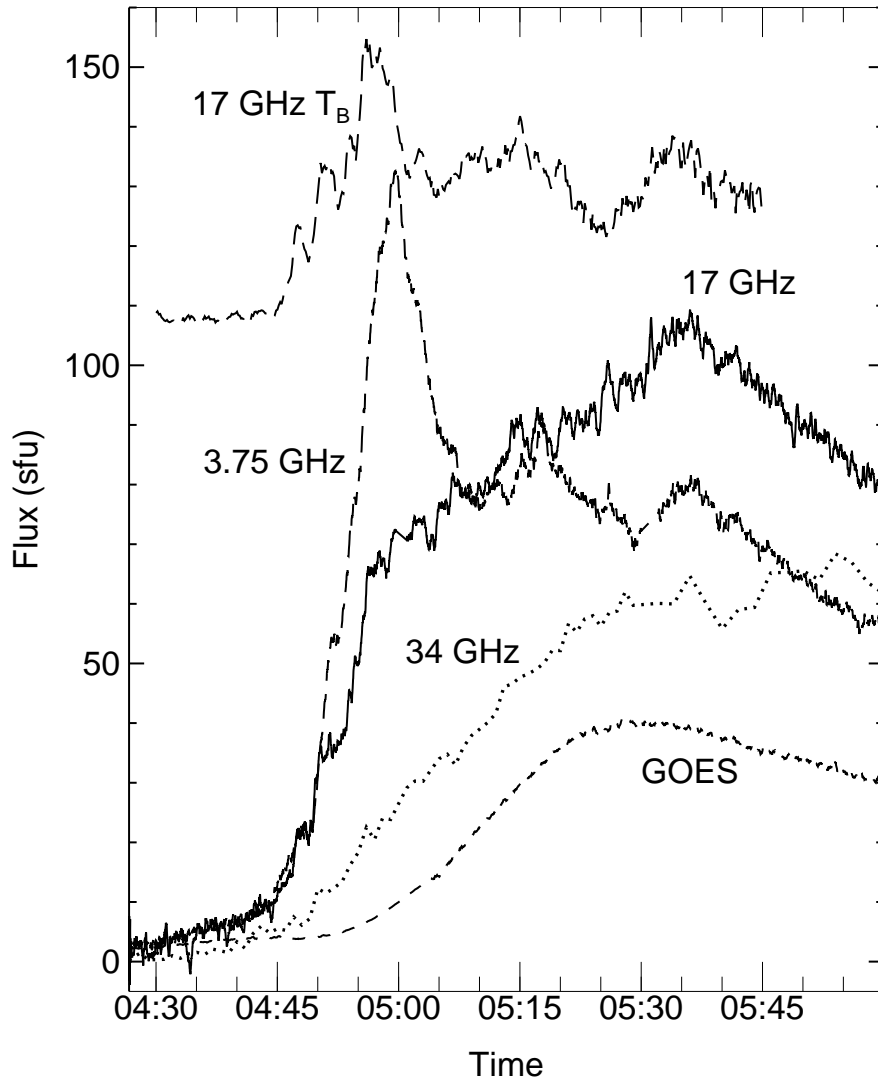


Fig. 6.— Light curves for the radio emission from the 2001 November 17 event at 3.75, 17 and 34 GHz, and the thermal free–free radio flux predicted from the GOES soft X–ray data. The 3.75 (long dashes) and 17 GHz (solid line) fluxes are from the Nobeyama Radio Polarimeters, while the 34 GHz fluxes (dotted line) are obtained from NoRH images. Curves are labelled by the frequency. The curve labelled “17 GHz T_B ” (long dashes) is the maximum brightness temperature from the 17 GHz maps (divided by 40000 and offset by 200) and is a proxy for the flux of the northern sunspot source in the flaring active region at 17 GHz. The total flux at the higher frequencies exhibits a gradual rise and then slow decay: at these frequencies the radio emission is dominated by thermal bremsstrahlung from the extended post–flare loops (see Fig. 7). The curve labelled “GOES” (short dashes) is the radio flux predicted by calculating the optically thin thermal bremsstrahlung from a plasma with the temperature and emission measure derived from background–subtracted GOES data via the goes routine in the SolarSoft IDL software package.

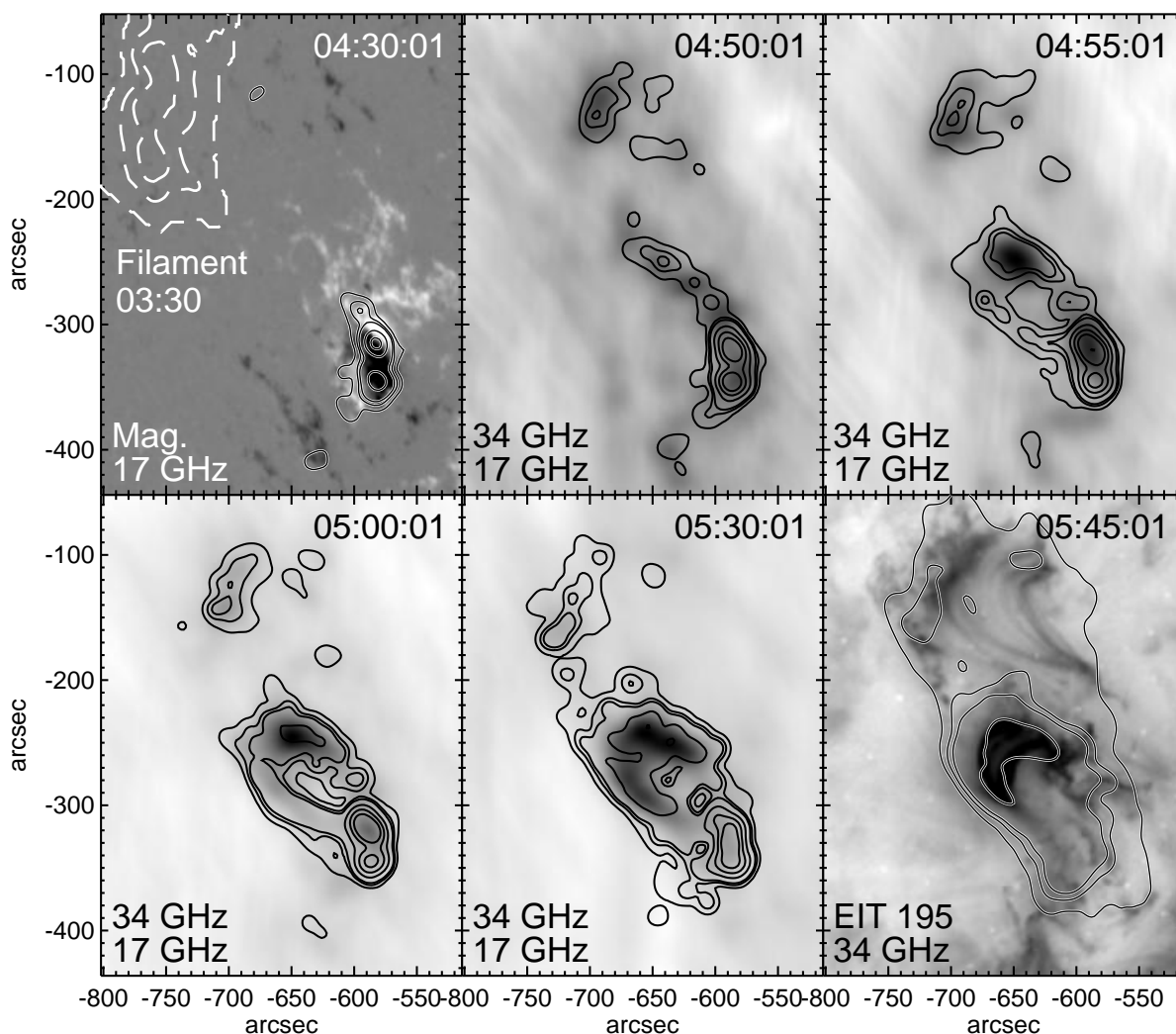


Fig. 7.— A sequence of NoRH radio images of the flare in the active region to the south–west of the filament. The first panel shows contours (solid) of the 17 GHz emission at 04:30 UT overlaid on a magnetogram from the Michelson Doppler Interferometer (MDI) on SOHO, acquired at 04:48 UT. The dashed white contours indicate the location of the filament prior to the onset of motion, from the 34 GHz image at 03:30 UT. The next 4 panels show contours of the 17 GHz emission overlaid on a greyscale image of the 34 GHz emission at the times indicated. In the last panel the greyscale image is an EIT 195 Å image at 05:48 UT and the contours represent the 34 GHz emission at 05:45 UT. Contour levels are at 2, 4, 6, 20, 50, 100, 300 & 1000 $\times 10^4$ K at 17 GHz and 0.4 times these levels at 34 GHz. The double radio source in the bottom right corner of the panels is located over the sunspots in the active region. The main flare loop, also seen in the SXI images of Fig. 4, is coincident in the radio and EIT images.